ChemComm

Accepted Manuscript

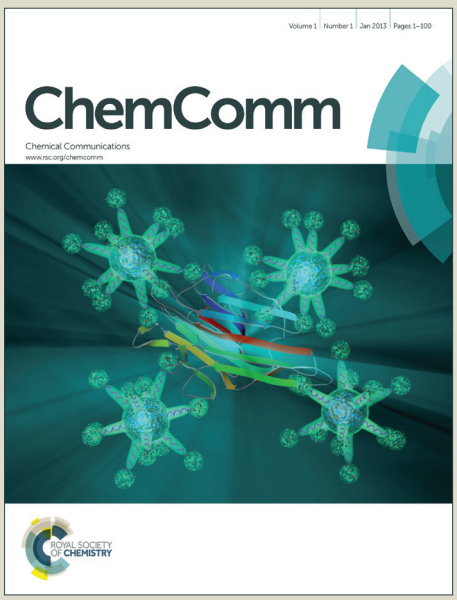

ROYAL SOCIETY OF CHEMISTRY

www.rsc.org/chemcomm

Cite this: DOI: 10.1039/c0xx00000x

www.rsc.org/xxxxxx

COMMUNICATION

Microplasma-Chemical Synthesis and Tunable Real-time Plasmonic Responses of Alloyed Au_xAg_{1-x} Nanoparticles

Tingting Yan,[a] Xiao Xia Zhong,[*a] Amanda Evelyn Rider,[b,c] Yi Lu,[a] Scott A. Furman,[b] and Kostya (Ken) Ostrikov[*b,c,d]

Received (in XXX, XXX) Xth XXXXXXXXX 20XX, Accepted Xth XXXXXXXXX 20XX
DOI: 10.1039/b000000x

Tunable synthesis of bimetallic Au_xAg_{1-x} alloyed nanoparticles and *in situ* monitoring of their plasmonic responses is presented. This is a new conceptual approach based on green and energy efficient, reactive, highly-non-equilibrium microplasma chemistry.

Due to the tunability of their properties, metal alloyed nanoparticles (NPs) are of interest for novel applications in plasmonics, catalysis, nanomedicine, medical imaging, cancer treatment, etc. [1-7] By changing the nanoparticle size, composition and/or the distribution of the elements within the NP (i.e., internal structure – either a homogenous composition throughout the NP, a smooth compositional gradient or a core and a number of discrete shells),[8-10] different properties may be obtained. Two examples of promising bimetallic alloys include Al_xFe_y which is a low-cost candidate for the replacement of Pd as a catalyst for heterogeneous hydrogenation[11] and Ni_xFe_{1-x} NPs synthesized via microplasma[12] for the chirality control of carbon nanotubes.

Noble metal alloyed NPs[13] such as Au_xAg_{1-x},[10,14-19] are extensively investigated for plasmonics-related applications,[10,17-19] catalysis[20-22] and biosensing,[23] as they exhibit tunable properties between the values for pure Au and pure Ag.[14] The NP structure (i.e., whether it is core-shell or a well-mixed bimetallic alloy) determines its application. In some cases, Au core-Ag shell NPs can be transformed into AuAg alloy NPs by annealing them at 250 ^oC.[14] However, it is still quite difficult to control the growth of Au_xAg_{1-x} NPs to ensure it is a well-mixed, crystalline alloy from the earliest possible growth stages.

Current colloidal chemistry synthesis methods of Au_xAg_{1-x} alloy NPs involve either standard chemical approaches, i.e., reducing gold and silver salts in solution in the presence of a reducing agent such as $NaBH_4$ and a capping agent (e.g., citrate),[15] or replacement reactions, which is a complex, multistep process involving elevated temperatures (up to 100^oC) and the presence of $NaBH_4$.[16] These methods have a number of drawbacks, e.g. the toxic nature of the reducing agent and the necessity to remove capping agents which can contaminate the surface (often irreversibly) with many impurities. Moreover, complicated multi-step processes are less viable for industrial applications, and high temperatures increase the energy cost of the process. These factors make *in situ* UV-Vis absorption monitoring (indispensable for controlling the NP characteristics from the earliest growth stages) exceedingly difficult, and in cases where annealing is involved, simply not possible.

We present a viable alternative for the green, energy-efficient synthesis of bimetallic alloyed nanoparticles. This is a new conceptual approach based on reactive, highly non-equilibrium plasma chemistry.[24-26] Our microplasma-chemical synthesis, in particular, presents an attractive alternative to the above-mentioned methods. Microplasmas feature at least one dimension in the sub-mm range[27] (see ESI Section S7 for more information on the microplasma characteristics). They have been used for a range of applications from bacterial inactivation, through to nanoparticle synthesis both in the gas[12] and liquid phase.[28] In the synthesis of metal nanoparticles in the liquid phase, a microplasma is used as the cathode, a metal salt/stabilizer mixture

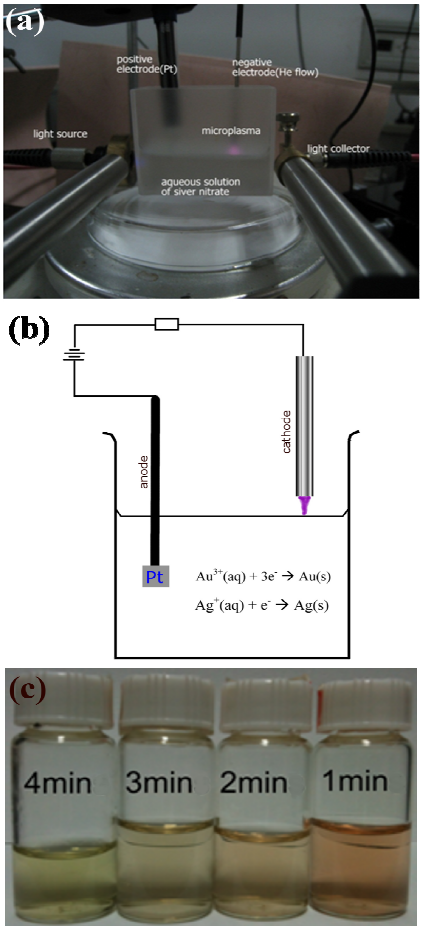

Fig. 1. (a) Photograph of *in situ* monitoring set-up for the synthesis of nanoparticles, (b) diagram of the plasma-chemical set-up used to synthesize Au_xAg_{1-x} alloy NPs. (c) Photograph of colloidal Au_xAg_{1-x} NP solutions for 1 – 4 min process times.

is used as the electrolyte and a metal foil as the anode (see Fig. 1(a-b) and ESI Section S1). The metal foil can either take part in the synthesis (i.e., it is oxidized, providing metal ions which are then reduced at the cathode) or be an inert electrode (i.e., Pt), with the metal salt in the electrolyte providing the material for the NP synthesis. Here we use the latter case, where only the metal salt in the electrolyte contributes to the nanoparticle growth.

The advantage of using a microplasma to co-reduce Au and Ag salts ($HAuCl_4$ and $AgNO_3$, in this case), is that it is a comparatively *green process*, i.e., there is no need for reducing agents such as $NaBH_4$, citrate or hydrazine as the plasma generates electrons (and also ions and excited radicals). Whilst the microplasma considered here is fairly chemically simple, it induces *multiple* reaction pathways for the synthesis of nanoparticles, from the standard dissociation and subsequent reduction reactions of metal salts that occur in colloidal synthesis as well as more exotic radical-induced reactions[29-31] (see ESI, Section S7). Microplasma-assisted electrochemical synthesis is a fast process, taking only minutes due to the energetic plasma electrons (see Fig. 1(c)) whereas many traditional chemical processes can often take hours/days. Moreover, it is a more energy efficient process than synthesis methods requiring heating (e.g., by at least a factor of 10, most likely considerably more than the common citrate method, see ESI Section S2). There is also a higher degree of control over the nanoparticle surface chemistry, with no undesired surface products that need to be removed, as in the case where more complex chemical mixtures are used. The main difference between the plasma-assisted method and other similar approaches (UV-, microwave-, and ultrasound-assisted), is the type of reaction-inducing agents, namely electrons, ions, and excited radicals in our case, whereas light, microwaves, and ultrasonic waves are used for UV-, microwave-, and ultrasound-assisted techniques, respectively (see ESI, Section S8).

Here we present the liquid-phase synthesis of Au_xAg_{1-x} alloyed NPs via microplasma-induced co-reduction of metallic ions and more exotic radical induced reactions. These additional, enhanced (compared to conventional colloidal chemistry) reaction pathways, coupled with the higher energy of the plasma-generated electrons lead to much faster formation of the Au_xAg_{1-x} nanoparticles. Moreover, this is a single-step process, at ambient conditions (i.e., room temperature and atmospheric pressure), with *in situ* monitoring of NP growth easily incorporated into the experimental set-up (see Fig. 1 (b)), which provides real-time information about the characteristics of the NPs as they are forming. It is shown that the composition of the NPs is tunable by varying the reaction time. Hence, the effective, non-equilibrium reactive plasma chemistry represents a viable, low-cost, and highly promising green approach for the energy-efficient and potentially scalable synthesis of a range of alloyed nanoparticles.

A transmission electron micrograph (TEM) of the synthesized $Au_{1-x}Ag_x$ NPs for 2 minutes processing time with the corresponding particle size distributions (PSD, taken over a number of TEMs, fit to a Gaussian distribution) is presented in Fig. 2 (a-b) [more TEMs and PSD are provided in the ESI, Section S3]. Fig. 2(c) summarizes the data obtained from the TEMs for the 1 – 4 min samples. It is clear from Fig. 2(a) that the NPs are fairly uniform, both in size and shape. As seen from Fig. 2(c), generally, as processing time increases, the peak of the PSD increases from 10.1 to 13.3 nm, whilst the full width at half maximum (FWHM, roughly, a measure of the size uniformity of the NP yield) increases from 4.2 to 5.1 nm.

Figs. 3 (a-d) show high-resolution TEMs and selected area electron diffraction (SAED) patterns, taken from samples prepared at 1, 2, 3, and 4 min., respectively. It should be noted that no core-shell structure is discernable from the HR-TEMs (see possible interpretations in ESI, Section S3). This data shows that it is possible to control crystal structure by varying the growth time. For example, for the 4 min sample (Fig. 3 (d)), it is clear that the particles are polycrystalline. The measured lattice spacing of 0.2357 nm and 0.2040 nm fall in between the Au and Ag values for (111) and (200) planes, respectively [(111): Ag = 0.2359 nm, Au = 0.2350; (200): Ag = 0.2044 nm, Au = 0.2030 nm]. We emphasize that these alloys were crystalline prior to exposure to an electron beam during HR-TEM analysis. This conclusion is also supported by X-ray diffraction spectra provided in the ESI Section S4.

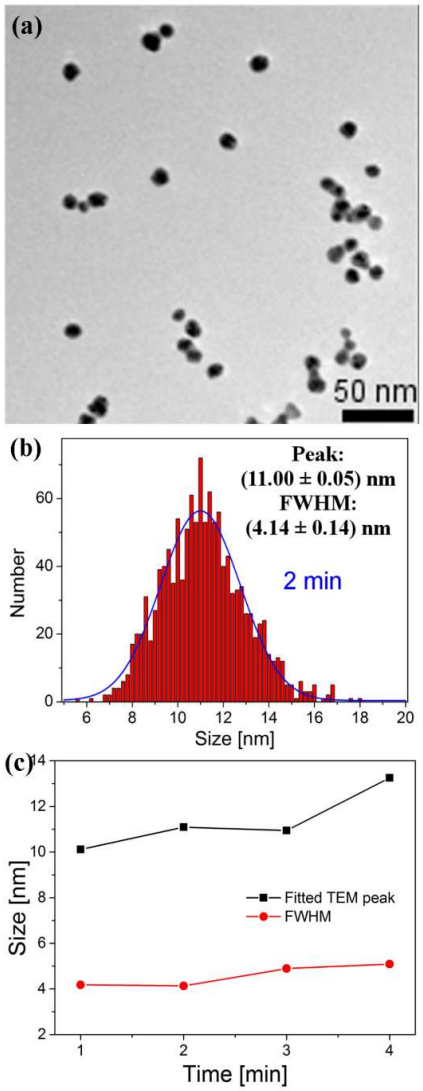

Fig. 2. TEM (a) and PSD (b) of Au_xAg_{1-x} alloy NPs produced using a microplasma exposure of 2 min. (c) Summary of size/PSD information from TEMs.

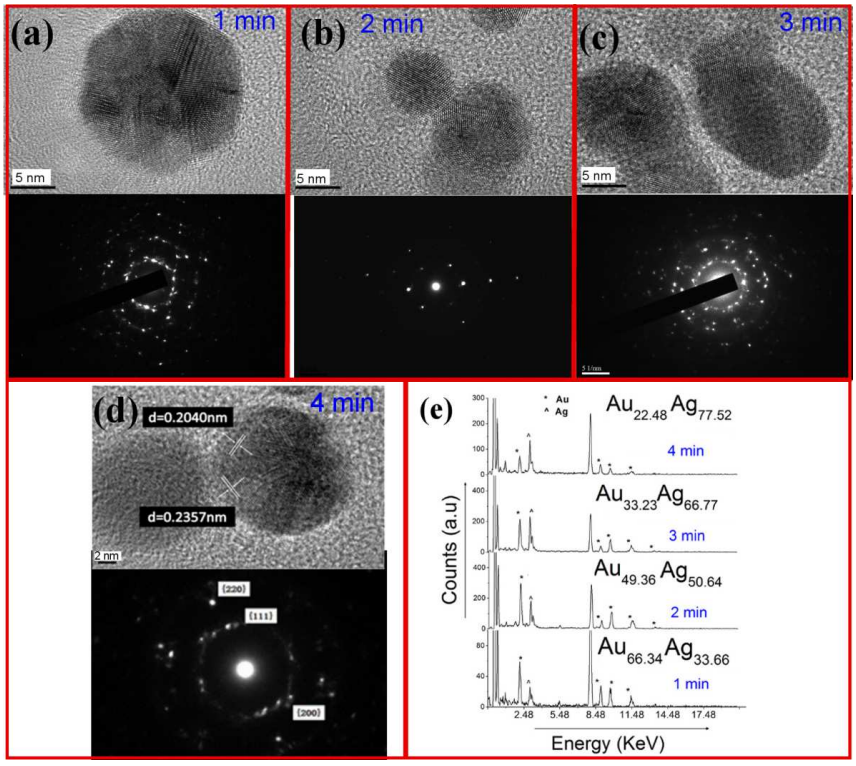

Fig. 3. High-resolution TEMs and selected area electron diffraction patterns of Au_xAg_{1-x} alloy NPs produced using a microplasma exposure time of (a) 1 min, (b) 2 min, (c) 3 min and (d) 4 min. (e) EDX spectra of Au_xAg_{1-x} alloy NPs at different exposure times

Energy dispersive X-ray (EDX) spectra are provided in Fig. 3(e), showing that the silver content increases for longer processing times. Specifically, by comparing the ratio of the AgK_α and AuK_α lines in the EDX spectra, the ratio of Ag:Au was determined to be 34:66, 51:49, 67:33, 78:22 after 1, 2, 3, and 4 min processing time, respectively. Once the NP composition is known, one can use the Vegard's Law to determine the lattice constant of the alloy

$$a_{AuAg} = xa_{Au} + (1\text{-}x)a_{Ag}, \qquad (1)$$

which depends linearly on the lattice constants of the individual metal components, a_{Au} and a_{Ag}. This gives nearly an exact match to the measured values of 0.2357 nm and 0.2040 nm from the (111) and (200) planes observed on the SAED pattern for the 4 minute sample. A small addition of Au led to a decrease in the lattice spacing away from pure Ag. Quite different SAED patterns were obtained for different processing times. Hence, combined with the HR-TEMs, XRD and EDX, we can conclude that both crystallinity and composition can be controlled by simply varying the reaction time.

Let us now consider Fig. 1(c) which shows the color change of the colloidal solutions with processing time. Once the atmospheric-pressure microplasma impinges on the surface of the solution, the colorless solution first turns reddish, indicating the AuAg nanoparticles are forming. With increased processing time, the solution turns greenish, which indicates an increased amount of silver in the NPs. This conclusion is supported by the corresponding UV-Vis spectra (Fig. 4 (a)) which shows a blue shift with increased time, e.g. from 486 to 403 nm as time increases from 1 to 4 minutes. This can be explained by considering the half cell reactions for Au and Ag:

$$Au^{3+}(aq) + 3e^- \rightarrow Au(s) \qquad (2)$$

$$Ag^{+}(aq) + e^- \rightarrow Ag(s) \qquad (3)$$

The reduction potential for Au (E^o = 1.52 V) is higher than that for Ag (E^o = 0.799 V). This means that Au has a higher affinity for electrons, hence is likely to be reduced quicker than the Ag ions in the solution. This is supported by the observed initial appearance of a red color in the solution. With longer processing times, the Ag ions are still reduced, even after the Au ions have been consumed (the Au being in the solution at a reduced concentration, i.e. Au:Ag in solution was 1:4). The shape of the UV-Vis absorption spectra indicates that the produced NPs are indeed *bimetallic nano-alloys*.

This interpretation is supported by the experiments of Mallin et al.,[15] who noted that the appearance of 2 peaks in the UV-Vis absorption spectra is indicative of either mixed, single metal nanoparticles or, when the peaks vary in relation to each other, of core-shell nanoparticles. In contrast, a single peak can represent either single metal NPs or fairly well-mixed bimetallic nano-alloys. By considering the shape and location of the peaks in Fig. 4(a), we can rule out single-element NPs – thus reinforcing our conclusion that Au_xAg_{1-x} nano-alloys have been obtained.

By combining the UV-Vis data with the EDX data from Fig. 3(e) and the PSD from Fig. 2, we are able to link the UV-Vis data to processing time and composition data and hence determine that increased amounts of silver were present for larger processing times to produce larger NPs. Fig. 4 (b) shows that there is a clear linear relationship between the wavelength and the processing time, as well as the wavelength and nanoparticle composition (see ESI Section S5).

Therefore, we have demonstrated that well-mixed bimetallic alloys have reliably been obtained with the *x* values between 22 and 66. This method is also promising for other bimetallic alloy nanoparticles (see ESI Section S6 for preliminary results for AuPt NP alloys). The additional tuning of plasmonic responses in bimetallic nanoparticles (as compared to single-metal NPs) offers extra possibilities to utilize the electron charging and plasmonic effects in next-generation energy conversion devices such as dye-sensitized solar cells. Our process may be scalable by utilizing

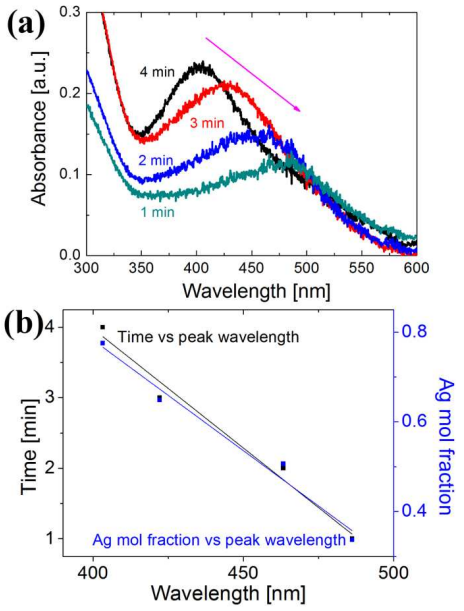

Fig 4. (a) UV-Vis absorbance spectra of samples produced with a 1 – 4 min exposure time; (b) graphs of time and Ag mol fraction (1-x) *versus* peak UV-Vis absorbance wavelength.

a line or 2D array of plasma jets or dielectric barrier discharges (DBD), and eventually flow-through techniques which is currently under investigation.

The reaction rates of reduction and NP formation in the vicinity of the plasma are increased due to the influx of energetic electrons (with the equivalent 'temperature' in the range of tens of thousands of degrees, which is much higher compared to the electrons generated using chemical reducing agents). The energy of the electrons may be tailored by varying the plasma parameters. This may enhance the Au and Ag reduction reactions and also increase diffusion rates near the plasma.[28] Plasma-generated electrons may also interact with the other species in the reaction volume (e.g., water), setting off a chain of reactions involving the creation of radicals[31] (e.g., hydrogen and hydroxyl) and culminating in the reduction of metal ions, which then form nanoparticle seed nuclei (see ESI, Section S7 for a discussion of plasma-specific effects[32,33]). Hence there are multiple additional, enhanced (compared to conventional physical chemistry) reaction pathways leading to the nanoparticle synthesis. A similar process conducted with the same reagent mixture and temperature but without any plasma, does not produce these nanoparticles.

In summary, we have presented a viable approach to alloyed bimetallic nanoparticle synthesis based on the effective, non-equilibrium reactive microplasma chemistry. In particular, we demonstrated a single-step, microplasma-chemical green synthesis of crystalline Au_xAg_{1-x} NP alloys in solution at ambient conditions, with the effective control over the size and composition of the NPs possible by variation of the reaction time. Alloyed noble metal nanoparticles such as these are promising as sensor components due to their tunable optical extinction. The ability to easily produce crystalline bimetallic alloyed NPs in favourable conditions with real-time monitoring will afford a greater degree of control over the NP characteristics and hence a superior product for implementation in a range of technological devices with precise specifications.

Notes and references

[a] *Shanghai Jiao Tong University, Shanghai 200240, P. R. China. E-mail: xxzhong@sjtu.edu.cn*

[b] *CSIRO Materials Science & Engineering, Lindfield, NSW 2070, Australia. E-mail: Kostya.Ostrikov@csiro.au*

[c] *Faculty of Science, The University of Sydney, NSW 2006, Australia;*

[d] *University of Technology Sydney, Broadway NSW 2007, Australia*

† Electronic Supplementary Information (ESI) available:[1. Experimental Details; 2. Estimate of energy required for microplasma versus citrate methods; 3. Au_xAg_{1-x} overview TEMs and PSDs; 4. X-ray diffraction spectra; 5. Peak fit for UV-Vis absorbance data; 6. Technique suitability to produce other alloys: AuPt; 7. A discussion of typical microplasma-species and plasma-related effects on nanoparticle formation and a proposed mechanism for Au_xAg_{1-x} nanoparticle formation in liquid via microplasma-assisted electrochemistry; 8. Comparison of microplasma-assisted and UV-, microwave-, and ultrasound-based methods and notes on potential applications.]. See DOI: 10.1039/b000000x/

1 Y. Chen, H. Cao, W. Shi, H. Liu, Y. Huang, *Chem. Commun*. 2013, **49**, 5013.
2 K. Shin, D. H. Kim, H. M. Lee, *ChemSusChem* 2013, **6**, 1044.
3 M. Sankar, N. Dimitratos, P. J. Miedziak, P. P. Wells, C. J. Kiely, G. J. Hutchings, *Chem Soc Rev* 2012, **41**, 8099.
4 Q. Liu, Z. Zhao, Y. Lin, P. Guo, S. Li, D.Pan, X. Ji, *Chem. Commun*. 2011, **47**, 964.
5 P. N. Njoki, L. V. Solomon, W. Wu, R. Alama, M. M. Maye, *Chem. Commun.* 2011,**47**, 10079.
6 X. W. Liu, X. G. Liu, *Angew. Chem. Int. Ed.* 2012, **51**, 3311.
7 A. K. Thapa, T. H. Shin, S. Ida, G. U. Sumanasekera, M. K. Sunkara, T. Ishihara, *J Power Sources* 2012, **220**, 211.
8 R. E. Bailey, S. Nie, *J. Am. Chem. Soc.* 2003, **125**, 7100.
9 R. Ferrando, J. Jellinek, R. L. Johnston, *Chem. Rev.* 2008, **108**, 845.
10 M. G. Blaber, M. D. Arnold, M. J. Ford, *J. Phys.: Condens. Matter.* 2010, **22**, 143201.
11 M. Armbrüster, et al., Y. Grin, *Nature Mater.* 2012, **11**, 690.
12 W-H. Chiang, R. M. Sankaran, *Nature Mater*. 2009, **8**, 882.
13 W. Chen, R. Yu, L. Li, A. Wang, Q. Peng, Y. Li, *Angew. Chem. Int. Ed.* 2010, **49**, 2917.
14 M. S. Shore, J. Wang, A. C. Johnston-Peck, A. L. Oldenburg, J. B. Tracy, *Small* 2011, **7**, 230.
15 M. P. Mallin, C. J. Murphy, *Nano Lett*. 2002, **2**, 1235.
16 Q. Zhang, J-Y. Lee, J. Yang, C. Boothroyd, J. Zhang, *Nanotechnology* 2007, **18**, 245605.
17 N. Harris, M. J. Ford, P. Mulvaney, M. B. Cortie, *Gold Bull*. 2008, **41/1**, 5.
18 M.B. Cortie, X. Xu, M.J. Ford, *Phys.Chem.Chem.Phys*. 2006,**8**, 3520.
19 J. Wilcoxon, *J. Phys. Chem. B* 2009, **113**, 2647.
20 T. Udayabhaskararoo, Y. Sun, N. Goswami, S. K. Pal, K. Balasubramanian, T. Pradeep, *Angew. Chem. Int. Ed.* 2012, **51**, 2155.
21 A-Q. Wang, J-H. Liu, S. D. Lin, T-S. Lin, C-Y. Mou, *J. Catal*. 2005, **233**, 186.
22 B. Xia, F. He, L. Li, *Langmuir* 2013, **29**, 4901.
23 X. Ren, X. Meng, F. F. Tang, *Sensors Actuat. B-Chem.* 2005, **110**, 358.
24 J. Zheng, R. Yang, L. Xie, J. Qu, Y. Liu, X. Li, *Adv. Mater.* 2010, **22**, 1451.
25 E. C. Neyts, A. C. T. van Duin, A. Bogaerts, *J. Am. Chem. Soc.* 2012, **134**, 1256.
26 M. Meyyappan, *J. Phys. D.: Appl. Phys.* 2009, **42**, 213001.
27 D. Mariotti, R. M. Sankaran, *J. Phys. D: Appl. Phys.* 2010, **43**, 323001.
28 X. Z. Huang, X. X. Zhong, Y. Lu, Y. S. Li, A. E. Rider, S. A. Furman, K. Ostrikov, *Nanotechnology* 2013, **24**, 095604
29 C. Richmonds, M. Witzke, B. Bartling, S. W. Lee, J. Wainright, C. Liu, R. M. Sankaran, *J. Am. Chem. Soc.* 2011, **133**, 17582.
30 J. Patel, L. Němcová, P. Maguire, W. G. Graham, D. Mariotti, *Nanotechnology* 2013, **24**, 245604
31 D. Mariotti, J. Patel, V. Svrcek, P. Maguire, *Plasma Proc. Polym.* 2012, **9**, 1074
32 M. Mozetic, U. Cvelbar, M. K. Sunkara, S. Vaddiraju, *Adv. Mater.* 2005, **17**, 2138
33 M G Kong, M Keidar, K Ostrikov, *J. Phys. D: Appl. Phys*. 2011, **44**, 174018.